Park, J., Lühr, H., Stolle, C., Rodriguez-Zuluaga, J. S., Knudsen, D. J., Burchill, J. K., Kwak, Y.-S. (2016): Statistical survey of nighttime midlatitude magnetic fluctuations: Their source location and Poynting flux as derived from the Swarm constellation. - *Journal of Geophysical Research*, *121*, 11, pp. 11,235—11,248.

DOI: http://doi.org/10.1002/2016JA023408

AGU PUBLICATIONS

JGR

Journal of Geophysical Research: Space Physics

RESEARCH ARTICLE
10.1002/2016JA023408

Key Points:
- During solstices the MMF Poynting flux is preferentially (but not always) from summer to winter hemisphere
- Magnitudes of the MMF Poynting flux peak around 2000-2100 MLT and are larger before midnight than after
- The magnitudes of the MMF Poynting flux is not well correlated with the undulation levels of in situ plasma density

Correspondence to:
J. Park,
pj@kasi.re.kr

Citation:
Park, J., H. Lühr, C. Stolle, J. Rodriguez-Zuluaga, D. J. Knudsen, J. K. Burchill, and Y.-S. Kwak (2016), Statistical survey of nighttime midlatitude magnetic fluctuations: Their source location and Poynting flux as derived from the Swarm constellation, *J. Geophys. Res. Space Physics*, *121*, 11,235–11,248, doi:10.1002/2016JA023408.

Received 30 AUG 2016
Accepted 11 OCT 2016
Accepted article online 14 OCT 2016
Published online 5 NOV 2016

Statistical survey of nighttime midlatitude magnetic fluctuations: Their source location and Poynting flux as derived from the Swarm constellation

Jaeheung Park[1,2], Hermann Lühr[3], Claudia Stolle[3,4], Juan Rodriguez-Zuluaga[3,4], David J. Knudsen[5], Johnathan K. Burchill[5], and Young-Sil Kwak[1,2]

[1]Korea Astronomy and Space Science Institute, Daejeon, Korea, [2]Department of Astronomy and Space Science, University of Science and Technology, Daejeon, Korea, [3]GFZ German Research Centre for Geosciences, Potsdam, Germany, [4]Faculty of Sciences, University of Potsdam, Potsdam, Germany, [5]Department of Physics and Astronomy, University of Calgary, Calgary, Alberta, Canada

Abstract This is the first statistical survey of field fluctuations related with medium-scale traveling ionospheric disturbances (MSTIDs), which considers magnetic field, electric field, and plasma density variations at the same time. Midlatitude electric fluctuations (MEFs) and midlatitude magnetic fluctuations (MMFs) observed in the nighttime topside ionosphere have generally been attributed to MSTIDs. Although the topic has been studied for several decades, statistical studies of the Poynting flux related with MEF/MMF/MSTID have not yet been conducted. In this study we make use of electric/magnetic field and plasma density observations by the European Space Agency's Swarm constellation to address the statistical behavior of the Poynting flux. We have found that (1) the Poynting flux is directed mainly from the summer to winter hemisphere, (2) its magnitude is larger before midnight than thereafter, and (3) the magnitude is not well correlated with fluctuation level of in situ plasma density. These results are discussed in the context of previous studies.

1. Introduction

Midlatitude electric fluctuation (MEF) and midlatitude magnetic fluctuation (MMF) are localized fluctuations of electric and magnetic fields, which can be observed by low-Earth orbit (LEO) satellites in the nightside midlatitude ionosphere. The first extensive study on this subject was done about 20 years ago by *Saito et al.* [1995]. In that paper statistical properties of MEFs were addressed, such as typical magnitude of a few mV/m and occurrence rate peaking at 0000–0200 in local time (LT). Some MEF examples accompanied with concomitant magnetic signatures (MMF) were also presented. Later, *Park et al.* [2009] conducted similar statistical studies of MMFs and reported that the MMF occurrence is (1) higher during solstitial seasons than during equinoxes and (2) higher before midnight than thereafter.

The source of MEF and MMF was generally attributed to medium-scale traveling ionospheric disturbances (MSTIDs) [*Yokoyama and Stolle*, 2016]. MSTIDs are band-like disturbances of ionospheric plasma at midlatitudes (see *Kelley* [2009, chapter 6] for a review of the phenomenon). *Saito et al.* [1998] and *Shiokawa et al.* [2003a] showed conjunction examples between ground-based observations of MSTID and satellite-based observations of MEF. *Park et al.* [2009] showed a case where MMFs appeared around an MSTID observed by a ground-based airglow imager. *Burke et al.* [2016] reported three passes of the Communications/Navigation Outage Forecasting System (C/NOFS) satellite, where a clear connection among MEF, MMF, and MSTID could be seen. *Park et al.* [2009, 2015] also supported close relationships between MMF and MSTID in a statistical sense, based on similar climatology (seasonal/longitudinal distribution) and morphology (preferred directions of the wavefronts) of the two phenomena.

MSTIDs are known to be conjugate across the equator like two mirror images [e.g., *Otsuka et al.*, 2004], but it has been expected that one of the hemispheres acts as a generator [e.g., *Martinis et al.*, 2010, sections 3.1–3.2]. It is generally accepted that MSTIDs are created by a coupling between the Perkins instability in the midlatitude *F* region [e.g., *Behnke*, 1979] and sporadic *E* instability in the connected *E* region [see *Cosgrove and Tsunoda*, 2004; *Tsunoda*, 2006; *Yokoyama et al.*, 2009]: for a concise review the readers are referred to *Kelley* [2009, chapter 6]. Then, one expects that MSTID generators (i.e., energy source) should be found preferentially

in the local summer hemisphere because the sporadic *E* occurrence rate is much higher during local summer than during local winter [see *Arras et al.*, 2008, Figure 3; *Arras*, 2010, Figure 6.7]. Considering the close relationship between MEF/MMF and MSTID, as mentioned above, we expect that the energy source of MEF/MMF should also exist in the summer hemisphere, leading to energy flow ($= \delta\vec{E} \times \delta\vec{B}/\mu_0$) from the summer to winter hemisphere. Actually, one conjugate MEF example discussed in *Saito et al.* [1995, Figure 5] supported the expectation.

In spite of the long history of extensive studies on MEF/MMF, it has not yet been statistically investigated as to what direction energy is transported to by the MEF/MMF (i.e., Poynting flux direction [e.g., *Kelley et al.*, 1991]) and with how much power (i.e., Poynting flux magnitude). *Saito et al.* [1995] analyzed *E* field data from the Dynamics Explorer 2 (DE-2) satellite, but its magnetometer had only limited sensitivity (noise level of a few nanoteslas). Hence, only the "signs" of Poynting flux (i.e., Poynting flux direction) for a few MEF events were addressed in that paper. *Park et al.* [2009] made use of the high-resolution *B* field data from the Challenging Mini-satellite Payload (CHAMP) satellite, but its *E* field (or equivalently, plasma drift velocity) probe (Digital Ion Drift Meter) was severely degraded during the launch, and the *E* field data are not available for scientific studies. *Burke et al.* [2016] calculated Poynting flux for MEF/MMF events and showed that the energy flows mainly from the summer to winter hemisphere with magnitudes of a few $\mu W/m^2$. But their study was limited to three consecutive passes of the C/NOFS on a single day, 17 February 2010. Therefore, the following question remains to be determined: what is the statistical behavior of the sign (e.g., summer to winter or winter to summer) and magnitude of Poynting flux associated with MEF/MMF? Further, *Burke et al.* [2016] observed fluctuations of in situ (at the C/NOFS position) plasma density along the MEF/MMF locations, but the correlation between the density fluctuation strength and Poynting flux was not addressed in depth. The statistical relationship between density fluctuation strength and Poynting flux magnitude is worth further investigation.

In this paper we address the statistical behavior of the sign and magnitude of Poynting flux from Swarm data for years 2013–2015. Furthermore, we investigate whether the magnitude of Poynting flux is related to the fluctuation amplitude of topside plasma density near the MEF/MMF locations. In section 2 the instruments and data processing method are briefly described. The statistical behavior of MMF Poynting flux is presented in section 3 and discussed in section 4. Finally, section 5 gives a summary of main findings and draws conclusions.

2. Instruments and Data Processing Methods

2.1. Instruments

On 22 November 2013 the European Space Agency (ESA) launched the Swarm constellation into a LEO orbit with an inclination angle of about 87.5° and an altitude of about 500 km. The constellation consists of three identically equipped satellites, which are termed Swarm-Alpha, Swarm-Bravo, and Swarm-Charlie. Between launch and the end of January 2014 all the three satellites were in a string-of-pearls configuration: that is, the three satellites were on nearly identical orbits with time lags of a few minutes in the order of Bravo, Alpha, and Charlie [e.g., *Lühr et al.*, 2015, Figure 1]. Between the end of January 2014 and April 2014 the three satellites conducted orbit maneuvers, and the final flight formation was achieved on 17 April 2014. In the final formation Swarm-Alpha and Swarm-Charlie fly side by side with a zonal separation of about 1.4° and north-south separation of about 50 km [e.g., *Xiong et al.*, 2016, Figure 1]. The stand-alone satellite, Swarm-Bravo, was put into an orbit with higher altitude (by about 50 km) and slightly higher inclination (by around 1°). The different inclination angle and different altitude of Swarm-Bravo make its orbital plane gradually separate from those of the other two (paired) satellites in terms of both LT and altitude. As of August 2016, Swarm-Bravo is about 4 h later in LT and 60 km higher in altitude than the satellite pair, Swarm-Alpha and Swarm-Charlie.

Each Swarm satellite is equipped with a Vector Field Magnetometer (VFM), an Absolute Scalar Magnetometer (ASM), Langmuir Probe (LP), and Thermal Ion Imager (TII) among other payloads. The VFM and ASM provide precise magnetic field vectors at a nominal cadence of 1 s. The LP measures electron density/temperature at a data rate of 2 Hz. The TII measures drift velocity vectors of ionospheric plasma twice a second, which can be transformed into *E* field assuming that the E × B drift dominates the ion motion. Therefore, both electric and magnetic fields can be observed by Swarm, which are essential for Poynting flux estimations. Due to concerns over anomalous background signal in the TII images, however, only a limited set of electric field measurements have been made public for validation purposes and for preliminary scientific study. A number of data quality issues have been noted for this data set (data identifier of "SW_PREL_EFI"), as stated in *Knudsen et al.* [2014]. Of particular relevance to this study are (1) the limited data coverage (mainly the period mid-April

through September 2014 for Swarm-Alpha and Swarm-Bravo only; data are available for all three satellites for approximately 2 weeks near the 2013 winter solstice and selected periods in the winter of 2015), and (2) the presence of large biases (offsets) which vary on orbital timescales (~90 min). Note that ion velocity (or equivalently, *E* field) measurements by LEO satellites are in general difficult because of the large bias term resulting from satellites' orbital speed (equivalent to 7.5 km/s in ion velocity or about 400 mV/m in *E* field strength).

The measurements also exhibit low signal-to-noise ratio particularly in regions of low plasma density. In spite of these issues, electric field variations on timescales faster than a few minutes are generally considered to be of good quality [e.g., *Archer et al.*, 2015; *Goodwin et al.*, 2015; *Fiori et al.*, 2016; *Juusola et al.*, 2016]. In this study we make use of the data from Swarm-Alpha and Swarm-Bravo, which are publicly available from https://earth.esa.int/web/guest/swarm/data-access.

No restriction is imposed in this study on geomagnetic activity: we use all the available Swarm data irrespective of the geomagnetic activity during the observation period. It is primarily because the data coverage of the Swarm/TII (the *E* field probe) is limited, as previously mentioned. Furthermore, the Swarm/TII data were mostly obtained during periods of low geomagnetic activity. The main body of the data is from the period, 15 April 2014 to 30 September 2014. The *Dst* during that period did not go below −80 nT. Thus, the statistical results in this study are not dominated by strong geomagnetic activity.

2.2. Data Processing Methods

The *E* field data quality of the Swarm/TII is still expected to be improved, and we use the magnetic field data observed by Swarm as a starting point of our analysis. We first search for MMF events in the Level-1b 1 Hz magnetic field data of Swarm-Alpha and Swarm-Bravo during nighttime (magnetic local time between 1800 and 0600) at low-latitude/midlatitude regions (magnetic latitudes within ±55°). We basically follow the MMF search method described in *Park et al.* [2015]. Figure 1 presents one example of MMF automatically detected by our data processing scheme. As a first step, we calculate the mean magnetic field which is calculated by applying a Savitzky-Golay low-pass filter (order 3, window size = 121 s ~ 900 km) to each component of the 1 Hz *B* field vectors. Then, the residual magnetic field is estimated by subtracting the mean magnetic field (background field approximated by the filter mentioned above) from the original data readings. As the original magnetic field vectors are given in the geographic North-East-Center (NEC) coordinate system, we transform the residual magnetic field into the mean field-aligned (MFA) frame: *z* (parallel) is along the mean magnetic field, *y* (zonal) is perpendicular to the mean magnetic field and horizontally pointing eastward, and *x* (meridional) completes the triad pointing outward to higher L shells. These residual magnetic fields in the MFA frame will be used for estimating Poynting flux. As a next step, the two transverse components (meridional and zonal: see Figures 1a and 1b) are further high-pass filtered by another Savitzky-Golay filter (order 3, window size = 25 s ~ 200 km) and rectified. Note that these signals out of the second high-pass filter will be used only for the purpose of MMF event detection: *not* for Poynting flux calculation. If the filtered/rectified signals (Figure 1f) are above 0.6 nT (the dashed horizontal line in Figure 1f), we mark them as MMF events (see the thick horizontal black bar in Figure 1f). However, we deem magnetic field fluctuations stronger than 10 nT as unphysical for nighttime midlatitude ionosphere: see the general strength (a few nanoteslas) of the MMF examples in *Saito et al.* [1995], *Park et al.* [2009, 2015], and *Burke et al.* [2016]. All MMF events with temporal separations of ≤30 s are grouped together (note that 30 s approximately correspond to 2° in latitude in Figure 1). The *z* (parallel or compressional) component of the residual magnetic field, after the same high-pass filter/rectification, should be below 0.1 nT (dashed horizontal line in Figure 1g) along the MMF event: otherwise, the MMF event is discarded. In this way we can avoid magnetic fluctuations associated with equatorial plasma bubbles (EPBs) [e.g., *Stolle et al.*, 2006]. Note that the 0.6 nT threshold (dashed horizontal line in Figure 1f) is slightly higher than the 0.4 nT used in *Park et al.* [2015]. Considering the limited number of available *E* field data, as mentioned above, we focus only on conspicuous MMF events and try to avoid weak fluctuations compromising the statistics.

As the 2 Hz *E* field (Swarm/TII) and electron density (Swarm/LP) data are not synchronized with the magnetic field data, we need to interpolate the former two data sets to the 1 Hz time stamps of the *B* field. Then, the *E* field is processed by the same procedure as that for *B* field: residual calculation by a Savitzky-Golay filter (order 3, window size = 121 s ~ 900 km) and coordinate transformation of residuals into MFA frame. The two *E* field

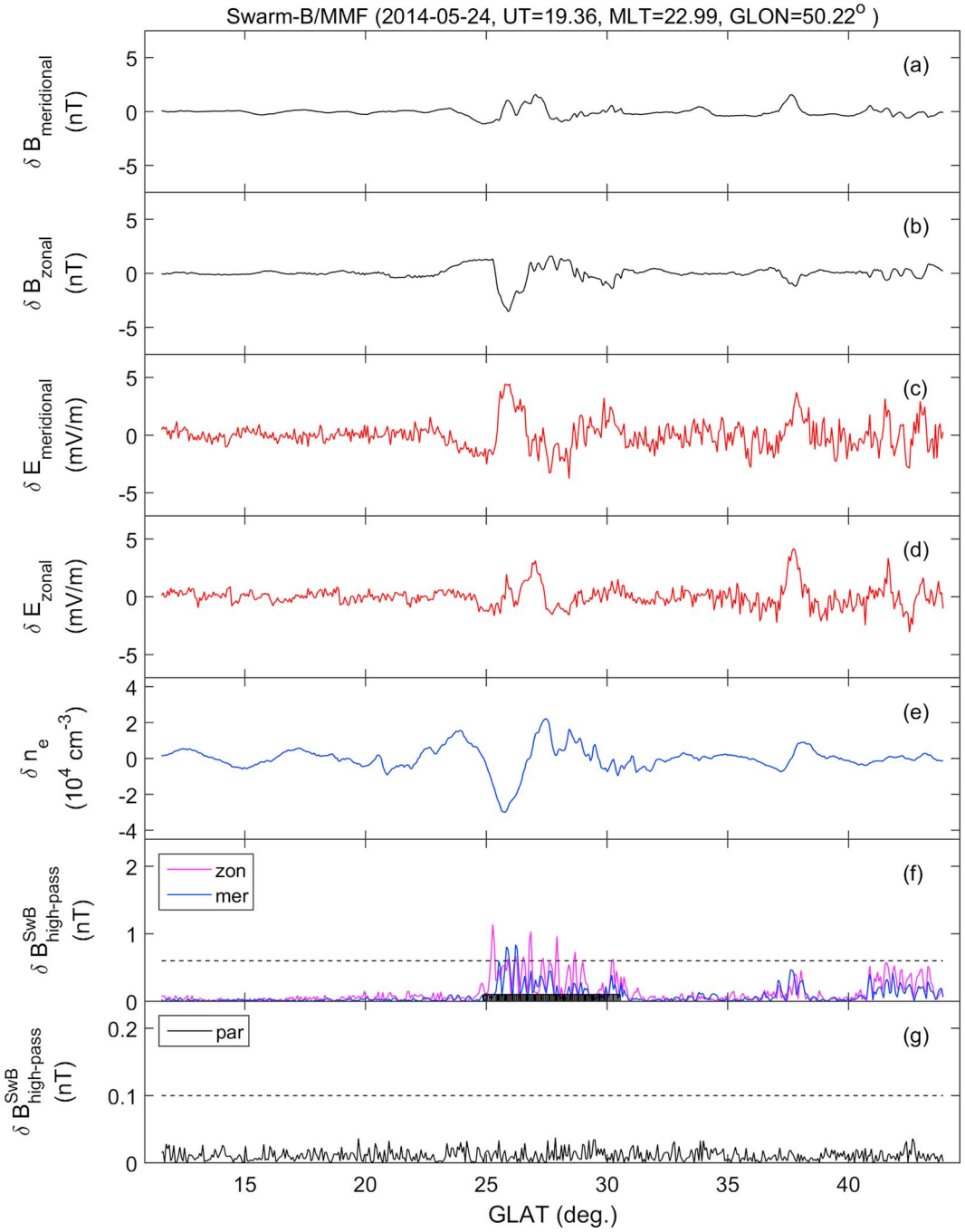

Figure 1. An example of MMF events demonstrating the automatic event detection and Poynting flux estimation: (a) δB_x (residual $B_{\text{meridional}}$), (b) δB_y (residual B_{zonal}), (c) δE_x (residual $E_{\text{meridional}}$), (d) δE_y (residual E_{zonal}), (e) δn_e (residual electron density), (f) filtered/rectified δB_x and δB_y, and (g) filtered/rectified δB_z (residual B_{parallel}). The dashed lines in Figures 1f and 1g represent threshold levels for accepting and discarding MMF events, respectively. The thick horizontal black bar in Figure 1f represents the MMF event interval detected automatically. For detailed information, see the text.

components perpendicular to the mean magnetic field (*x*/meridional and *y*/zonal) are shown in Figures 1c and 1d. The electron density residual (Figure 1e) is calculated in the same way, but no coordinate transformation is needed since it is a scalar.

We perform the following quality check of the *E* field data to avoid periods of unphysical Poynting flux associated with spurious *E* field signals. First, δE_x (Figure 1c) and δE_y (Figure 1d) should be below 10 mV/m. We deem electric field fluctuations larger than 10 mV/m as unphysical for nighttime midlatitude ionosphere:

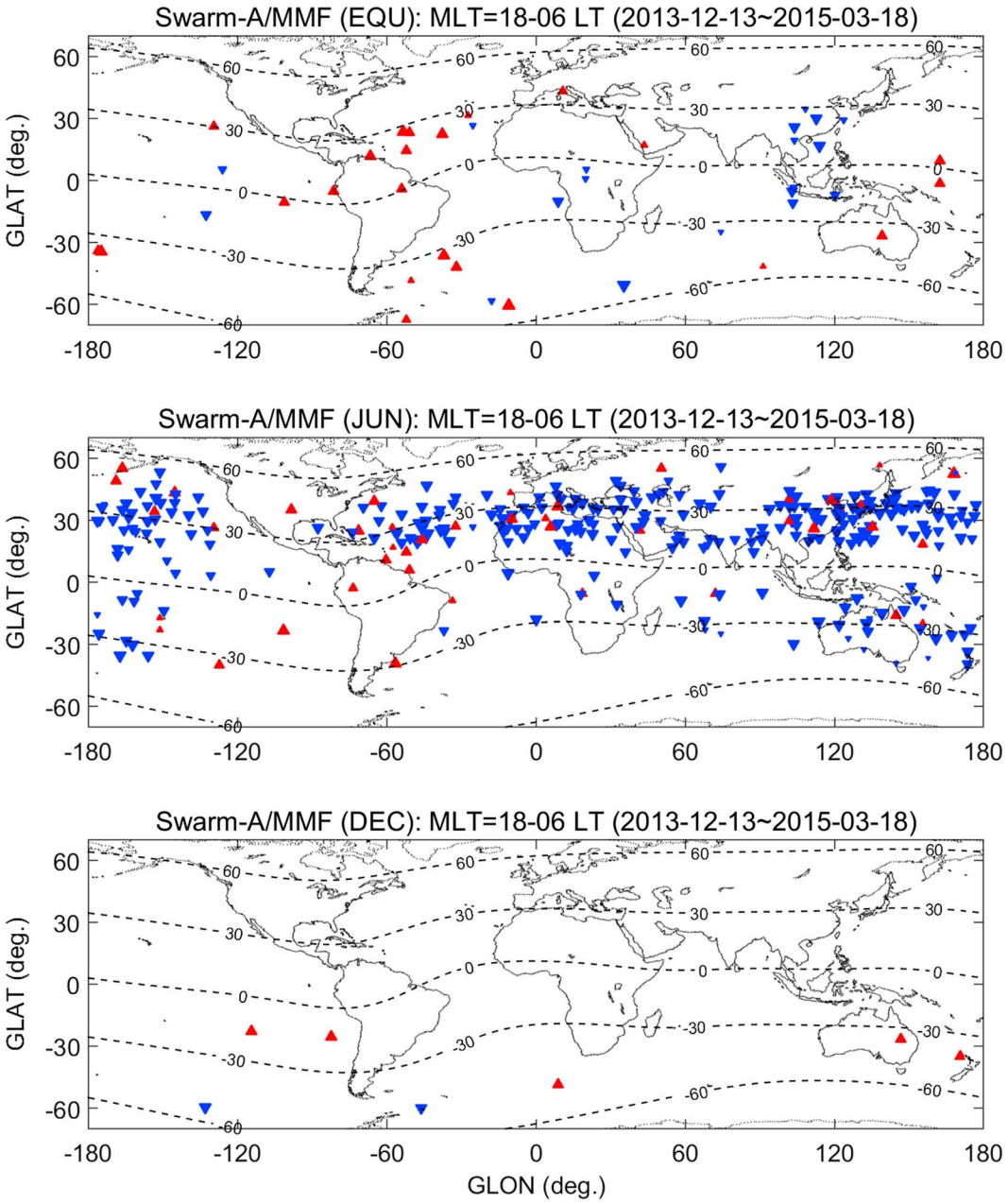

Figure 2. Geographic distributions of Swarm-Alpha MMF events identified by the automatic detection scheme described in section 2. The blue reverse (red forward) triangles represent southward (northward) Poynting flux with the sizes corresponding to the logarithm of Poynting flux magnitudes. (top to bottom) Equinox, June, and December seasons, respectively.

see MEF examples in *Saito et al.* [1995] and *Burke et al.* [2016]. The field-aligned component (z component in the MFA coordinate system) of Poynting flux is given by

$$S_z = \frac{1}{\mu_0} (\delta E_x \, \delta B_y - \delta E_y \, \delta B_x) \quad (1)$$

The paired components (e.g., δE_x and δB_y) are expected to show some correlations. Hence, our second criterion for the E field data is that the cross-correlation coefficients between δE_x and δB_y (or that between δE_y and δB_x) along an MMF event (±15 s margin) should be higher than +0.6 (positively correlated) or lower than −0.6 (anticorrelated) at their positive/negative extrema (i.e., with optimal time shift between E field and B field data). For example, if E field fluctuations exist both inside of an MMF event and outside, the E field fluctuations cannot be considered to be related with the MMF. In our data processing results the optimal time

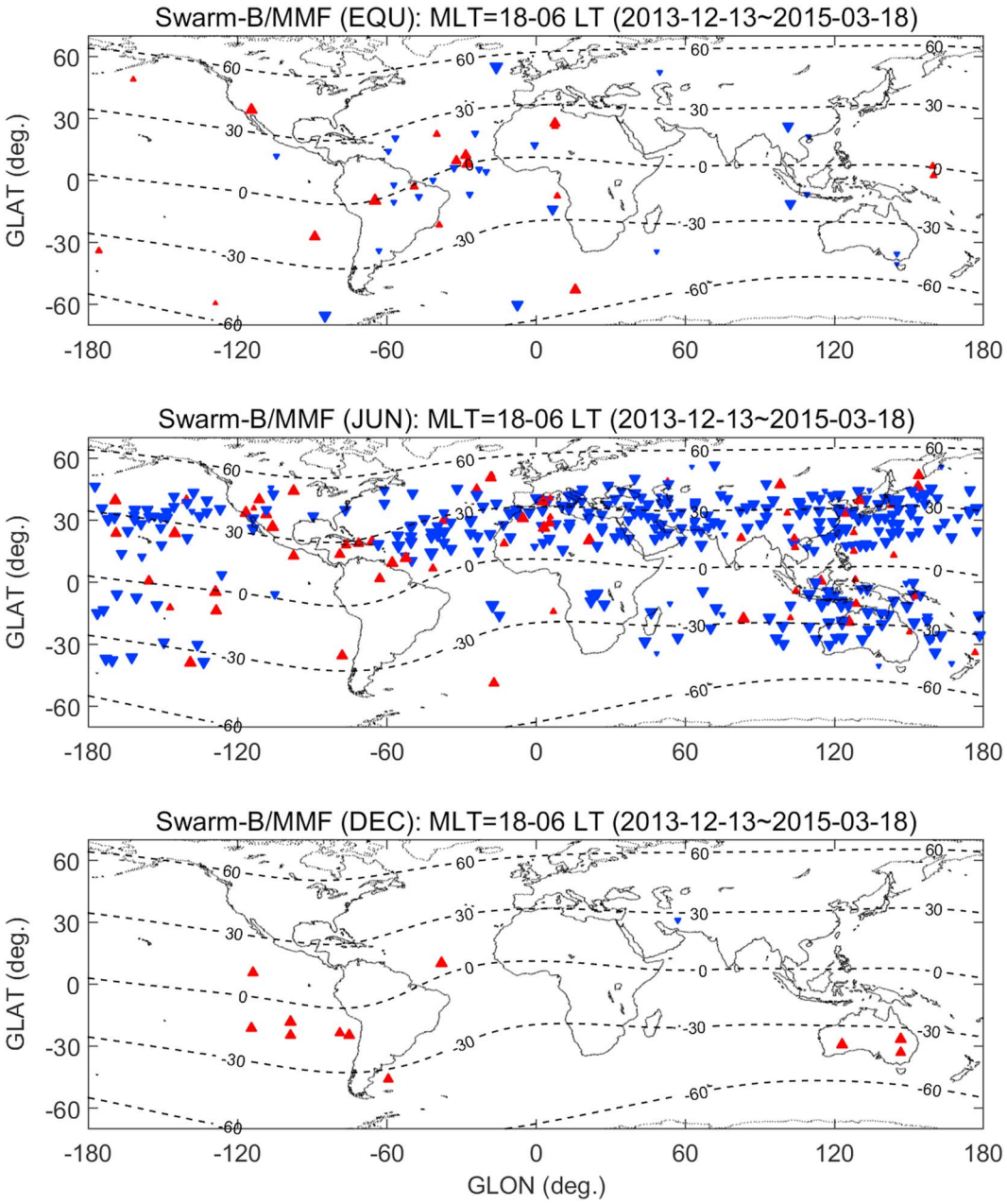

Figure 3. The same as Figure 2 but for Swarm-Bravo.

shift between *E* field and *B* field data is around zero in most cases. For Swarm-Alpha (Swarm-Bravo) the optimal time shift is within ±1 s for 77% (82%) of the MMF events. The small values of the optimal time shift are consistent with the properties of MEF examples in *Saito et al.* [1995] and *Burke et al.* [2016].

This somewhat restrictive criterion helps in selecting good-quality *E* field data and is consistent with the good correlations (positive or negative) between electric and magnetic fields reported for MEF and MMF [e.g., see *Saito et al.*, 1995, Figure 5a; *Burke et al.*, 2016, Figure 7]. With these criteria in mind, the statistical results in the following sections should be interpreted as the Poynting flux climatology of the MEF/MMF events "whose *E* field and *B* field profiles are well correlated with each other."

For every MMF event selected we calculate the field-aligned component of Poynting flux at 1 s cadence following equation (1) and average the value over the MMF interval (±15 s margin), in a way similar to that of *Hatch et al.* [2016, section 3]. This time-averaged Poynting flux (sign and magnitude) is recorded in the MMF

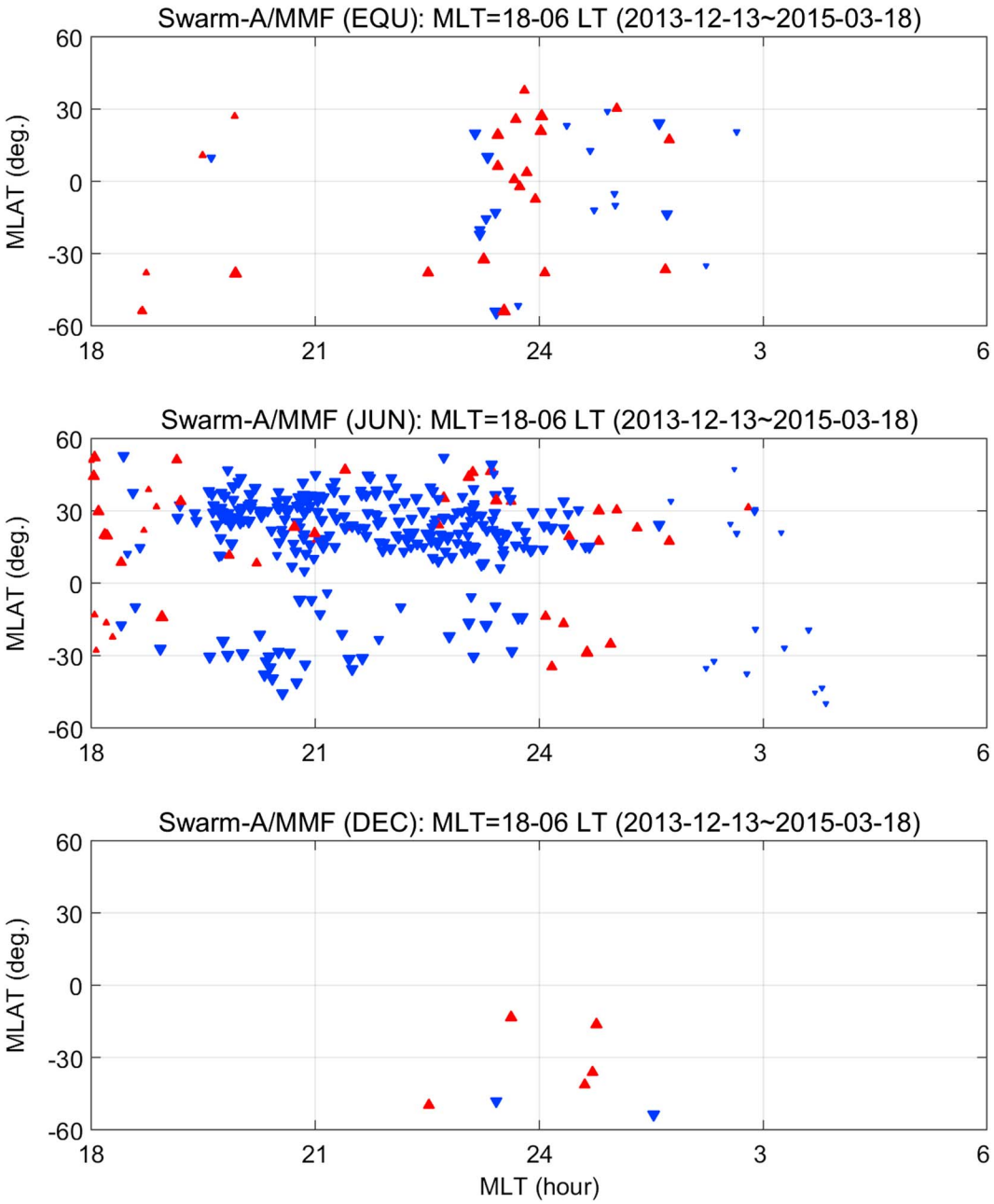

Figure 4. Distribution of Swarm-Alpha MMF events in the magnetic latitude (MLAT)-magnetic local time (MLT) frame. (top to bottom) Equinox, June, and December seasons, respectively.

event list and used for statistical studies. This value is about −2.2 μW/m^2 for the example in Figure 1: that is, the Poynting vector is directed from the Northern Hemisphere (NH) to the Southern Hemisphere (SH). As a next step, the standard deviation of plasma density residuals (Figure 1e) is calculated over the same MMF interval. Both the standard deviation itself ($\delta n_e^{\mathrm{stdev}}$) and the one normalized by the mean background plasma density ($\delta n_e^{\mathrm{stdev}}/n_e^{\mathrm{average}}$) are registered in the MMF event list for statistical analyses. These two values are about 1.3×10^4 cm^{-3} and ∼ 4%, respectively, for the example in Figure 1. Note in Figure 1e that the plasma density fluctuations do exist along the MEF/MMF, but the morphology of the former is not exactly the same as that of the latter. This feature agrees with the examples shown in *Burke et al.* [2016, Figure 4]. Note also that the diamagnetic effect (i.e., δB_z fluctuation [e.g., *Lühr et al.*, 2003]) of these plasma density fluctuations is safely below the threshold for MMF event rejection (see Figure 1g).

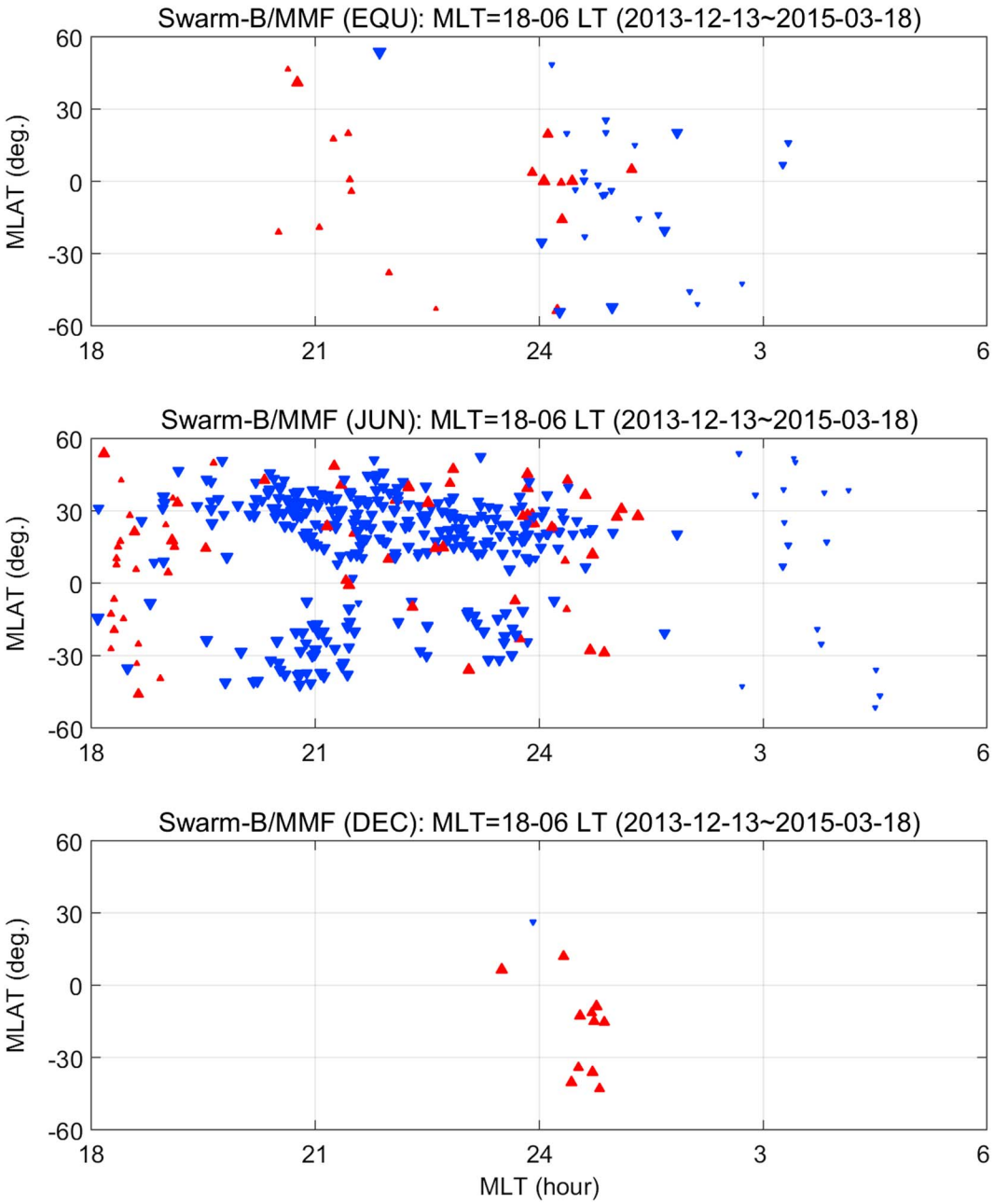

Figure 5. The same as Figure 4 but for Swarm-Bravo.

3. Statistical Results

Figure 2 shows the geographic and seasonal distribution of the *z* component (field-aligned component) of MMF-related Poynting flux as observed by Swarm-Alpha. Figure 2 (top to bottom) represents combined equinoxes (±32 days around 21 March and 21 September), June solstice (±65 days around 21 June), and December solstice (±65 days around 21 December). Each triangle corresponds to one MMF event. The direction and color of the triangles are related to the sign of the Poynting flux *z* component. Blue reverse triangles represent energy flow from the NH to the SH, and red upward triangles signify SH-to-NH energy flow. Sizes of triangles correspond to the logarithm of absolute magnitude of the Poynting flux *z* component: bigger symbols are for larger Poynting flux magnitude. Details of the absolute magnitudes will be shown later by other figures. The seasonal/geographical distribution generally agrees with the known MMF distribution as shown, for example, in *Park et al.* [2009, Figures 2–3]. During June solstice the MMF activity is high in the North

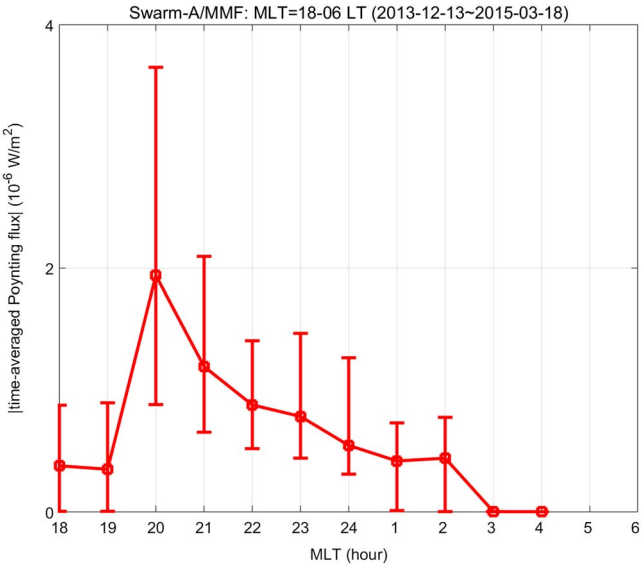

Figure 6. Magnitudes of time-averaged Poynting flux for Swarm-Alpha MMF events as a function of MLT. Square symbols represent median values, and the vertical bars represent upper and lower quartiles.

Atlantic, East Asia/Oceania, and North Africa/Europe. During December solstice only a few MMF events were selected because of the poor TII data coverage in this season, as mentioned in section 2. Note that Poynting flux cannot be calculated without the *E* field data from Swarm/TII. Nevertheless, the December solstice events are mostly around America and Pacific Ocean, which is consistent with *Park et al.* [2009, Figures 2–3]. From the reasonable agreement between Figure 2 and *Park et al.* [2009, Figures 2–3] we can see that our statistical analysis of MMF Poynting flux is not significantly biased to a certain subgroup of MMF events.

The Poynting flux direction in Figure 2 is generally (but not exclusively) summer to winter during solstices although there are only seven events in December solstice. During June solstice 284 MMF events (~87 % of the total) exhibit Poynting flux from summer (NH) to winter (SH) and 43 MMF events exhibit the opposite direction. Five of the MMF events during December solstice (~71% of the total) exhibited summer-to-winter direction and the two had the opposite. During equinoxes the Poynting flux is rather bidirectional with no preferred direction (23 MMF events with northward Poynting flux and 19 events southward). The magnitude of Poynting flux is not well organized by geographic locations or seasons. We cannot clearly tell whether Poynting flux magnitude during one season is notably larger than that of the other seasons.

Figure 3 is the same as Figure 2 but for Swarm-Bravo. The seasonal/geographical distributions are also consistent with a previous study by *Park et al.* [2009]. Especially, data coverage during December solstice is slightly better in Figure 3 than in Figure 2, and the MMF events are mostly around South America and Australia: this trend also agrees with *Park et al.* [2009, Figures 2–3]. The Poynting flux directions are again from summer to winter for most solstitial events. During June solstice 315 MMF events (~83% of the total) have summer-to-winter Poynting flux, and 65 events exhibited the opposite polarity. During December solstice 11 MMF events exhibit summer-to-winter Poynting flux, and 1 event has the opposite direction. During equinoxes the Poynting flux does not have a preferred direction but exhibits rather bidirectional behavior (18 MMF events with northward Poynting flux and 26 events southward).

Figure 4 is similar to Figure 2 showing Swarm-Alpha data, but the horizontal axis is magnetic local time (MLT), and the vertical axis is magnetic latitude (MLAT) instead of geographic latitude. Figure 5 is the same as Figure 4 but for Swarm-Bravo. June solstice is the only season with reasonable MLT coverage. During June solstice the Poynting flux magnitude is generally smaller right after sunset (~18 MLT) and early in the morning (~03 MLT) than in the other MLT sectors: this trend can be more easily seen in Figure 5 than in Figure 4. Between 1900 and 0200 MLT when the Poynting flux magnitude is large, the Poynting flux exhibits preference for summer-to-winter direction in Figures 4 and 5. Before 1900 MLT (after 0200 MLT), although the available data are limited to June solstice, winter-to-summer (summer-to-winter) direction seems to dominate in general.

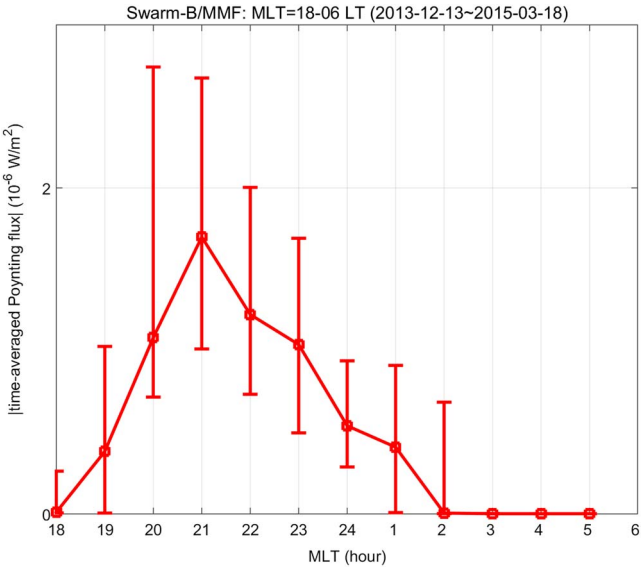

Figure 7. The same as Figure 6 but for Swarm-Bravo.

Figures 6 and 7 present the absolute magnitude of field-aligned Poynting flux (irrespective of sign) as a function of MLT for Swarm-Alpha and Swarm-Bravo, respectively. MMF events for all the three seasons are considered together for drawing these figures. The dots are median values within each 1 h MLT interval, and the vertical bars represent upper and lower quartiles. From the two figures it is clear that the Poynting flux before midnight is higher than that afterwards, in spite of the large interquartile ranges. The Poynting flux magnitudes estimated from Swarm-Alpha and Swarm-Bravo data are of the same order.

We further check the correlation of Poynting flux magnitude with absolute ($\delta n_e^{\text{stdev}}$) or relative ($\delta n_e^{\text{stdev}}/n_e^{\text{average}}$) standard deviation of residual plasma density (see Figure 1e) along each MMF event. We cannot identify any conspicuous relationship between the Poynting flux magnitude and the standard deviations of plasma density residuals (figure not shown). For Swarm-Alpha the correlation coefficient between the Poynting flux magnitude and the absolute and relative standard deviations of plasma density are 0.03 and 0.15, respectively. For Swarm-Bravo the two correlation coefficients are −0.06 and −0.03, respectively. As an alternative method of data processing, we calculate the correlation coefficient between the magnitude of $\delta n_e^{\text{stdev}}$ and that of Poynting flux for each MMF event. The median value of the correlation coefficients is also very low: 0.04 (0.06) for Swarm-Alpha (Swarm-Bravo). Even the correlation coefficients between the magnitude of $\delta n_e^{\text{stdev}}/n_e^{\text{average}}$ and that of Poynting flux for each MMF event have the median value of 0.04 (0.05) for Swarm-Alpha (Swarm-Bravo).

4. Discussion

4.1. Sign of the Poynting Flux

In section 3 we have shown that the field-aligned Poynting flux is directed preferentially from the summer to winter hemisphere, but not always. This result agrees with the case studies of *Saito et al.* [1995] and *Burke et al.* [2016]. *Saito et al.* [1995] reported that the conjugate MEF example in their Figure 5 (3 May 1982) exhibits summer-to-winter Poynting flux although the magnitude was not mentioned explicitly. *Saito et al.* [1995] also found that two MEF events observed within one day (on 27 August 1982) exhibited Poynting vector directions opposite to each other. Similarly, *Burke et al.* [2016] found that directions of the Poynting flux are mostly from summer to winter, but not always. *Burke et al.* [2016] interpreted the general summer-to-winter direction as supporting evidence for previous theories addressing MSTID generation in the summer hemisphere. The significant amount of exceptions (i.e., winter-to-summer Poynting flux) in our statistical study as well as in the case studies of *Burke et al.* [2016] may be attributed to nonzero occurrence of sporadic *E* layers in the winter hemisphere [see *Arras et al.*, 2008, Figure 3; *Arras*, 2010, Figure 6.7]. As the MSTID is generally thought to be generated by coupled Perkins and sporadic *E* instabilities, the existence of sporadic *E* in the winter hemisphere can result in energy flow (i.e., Poynting flux) from the winter to summer hemispheres. Another candidate mechanism for the winter-to-summer Poynting flux can be gravity waves (GWs) at midlatitudes in

the winter hemisphere [e.g., *Garcia et al.*, 2016, Figure 11]. When seed perturbations generated by winter GWs are strong enough, the growth rate of Perkins instability becomes higher even without coupling to sporadic *E* instability [*Tsunoda*, 2006, equation 33]. In that case the Poynting flux direction is expected to be from winter to summer.

Further, simulation work of *Yokoyama* [2014] demonstrated that the *F* region conditions (stability/instability) in the winter hemisphere is also important for MSTID generation in the summer hemisphere. The results imply that sporadic *E* layers in the summer hemisphere are coupled not only with the *F* region Perkins instability in the summer hemisphere but also with that in the winter hemisphere. This may be related with the nonzero occurrence of winter-to-summer Poynting flux of MMF events. Further theoretical studies are necessary to resolve this issue. Those studies on interhemispheric coupling should properly consider the nondipolar geometry of the terrestrial *B* field in interhemispheric *E* field mapping [e.g., *Martinis et al.*, 2010]. For example, the weak *B* field (i.e., diverging flux tubes) in the South Atlantic Anomaly can reduce the *E* field delivered from the conjugate hemisphere via field-aligned mapping of the electric potential.

Slight dominance of winter-to-summer Poynting flux right after sunset (~1800 MLT) is not well understood in the context of previous studies. For example, the sporadic *E*, which is generally deemed as a MSTID generator, preferentially occurs in the summer hemisphere in all MLT sectors [see *Arras*, 2010, Figure 6.7]. We speculate that as local sunset in the "summer" midlatitudes occurs significantly later than 1800 MLT, the persisting daytime condition around 1800 MLT may hinder the growth of *F* region plasma irregularities. Note that most of the theoretical works on MSTIDs assumed nighttime conditions [e.g., *Tsunoda*, 2006]. On the contrary, sunset in the "winter" hemisphere is before 1800 MLT, which should be more favorable for MSTID generation than the (still sunlit) summer hemispheric environments. As a result, the electromagnetic energy generated in the winter hemisphere may flow toward the summer hemisphere around 1800 MLT. However, we cannot draw firm conclusions from the limited amount of Swarm/TII data set available up to now and defer a definitive conclusion to a future study.

Finally, it is worth to point out that some MMF events in Figures 4 and 5 occur close to the magnetic equator. Those events may originate either (1) from EPBs whose diamagnetic signals are so weak that they are not filtered out by the selection criteria described in section 2 or (2) from MSTID/MMF events that have migrated toward the equator [e.g., *Makela et al.*, 2010]. As EPBs and MSTIDs are known to have different generation mechanisms (and related energy flow or Poynting flux directions), a possible existence of EPBs in our event list may compromise our conclusions on the Poynting flux. Fortunately, most of our MMF events are located poleward of ±15° MLAT, i.e., poleward of known EPB activity peaks [see, *Stolle et al.*, 2006; *Xiong et al.*, 2010]. Therefore, possible contamination by EPB events is expected to be minimal.

4.2. Magnitude of the Poynting Flux

In section 3 the magnitude of the field-aligned Poynting flux is generally larger before midnight than early in the morning. This result also supports the case studies of *Burke et al.* [2016], who reported that the observed Poynting flux gradually decreased with LT. The near-midnight peak of MEF [*Saito et al.*, 1995, Figure 7] and premidnight peak of MMF [*Park et al.*, 2009, Figures 2–3] can work together resulting in Poynting fluxes higher before midnight than after. This MLT asymmetry of Poynting flux is also consistent with the climatology of sporadic *E* (a generally accepted source of MSTID/MEF/MMF) shown in *Arras* [2010, Figure 6.7], where its premidnight occurrence is larger than postmidnight occurrence.

Note that the MLT dependence of our results may be aliased by seasonal variation of Poynting flux. MMF events constituting Figures 6 and 7 are dominated by June solstice observations, due to incomplete data coverage during equinoxes and December solstice. Additionally, all the June solstice data of Swarm/TII come from the year 2014. Swarm orbital planes were around 23 MLT in May 2014, around 20 MLT in June 2014, around 05 MLT in July 2014, and near 02 MLT in August 2014. That is to say, MLT changes are not fully decoupled from seasonal variation in our data set. Future studies with longer data sets can better separate the MLT dependence from seasonal variations of the Poynting flux.

According to Figures 6 and 7, the Poynting flux magnitudes for Swarm-Alpha and Swarm-Bravo data are of the same order. This is as expected if we assume that energy is conserved during its flow along a flux tube. *B* field strength of a dipole geomagnetic field is inversely proportional to the cube of the distance from the Earth's center. As *B* field strength is inversely proportional to flux tube area, we can expect that the ratio of the Poynting flux observed by Swarm-Bravo (altitude ~520 km) to that by Swarm-Alpha (altitude ~470 km) should be

$(6371.2\text{km} + 470\text{km})^3/(6371.2\text{km} + 520\text{km})^3 \sim 97.84\%$ during the formation flight phase. Here the Earth's radius is assumed to be 6371.2 km. During the initial commissioning phase, when all the three satellites were at the same altitude of about 500 km, the ratio should be identically 100%. In summary, we expect practically the same magnitudes of Poynting flux for Swarm-Alpha and Swarm-Bravo. The mean values of all the absolute Poynting flux observed by Swarm-Bravo and Swarm-Alpha are $1.30 \pm 1.46\mu\text{W/m}^2$ and $1.29 \pm 1.37\mu\text{W/m}^2$, respectively. The observation results roughly agree with the theoretical expectation that the Poynting flux magnitudes observed by the two Swarm satellites should not be very different. Furthermore, the magnitudes (a few $\mu\text{W/m}^2$) are of the same order as the values given in *Burke et al.* [2016, Figure 7]. The agreement provides a rough validation of the magnitudes of the variations in the Swarm filtered *E* fields on timescales up to a minute. On-going calibration work on the *E* field data [e.g., *Fiori et al.*, 2016] and precise magnetic field models that can be used for defining residual magnetic field may help to obtain reliable absolute values of the Poynting flux. This will be left for future work.

4.3. Magnitude of the Poynting Flux Versus MSTID Strength

Shiokawa et al. [2003b] reported that MSTID strengths around Japan decrease after midnight, which is in general agreement with the MLT asymmetries of Poynting flux magnitudes in our Figures 6 and 7. This result seems to support a certain relationship between the former and the latter. However, we can also find counterexamples in previous papers. For example, MSTID detection rates at some other observatories (e.g., in Europe) can be lower before midnight than after [see *Amorim et al.*, 2011, Figure 6; *Hernández-Pajares et al.*, 2012, Figure 10; *Otsuka et al.*, 2013, Figure 3]. The MSTID detection rates are expected to represent MSTID strengths to a certain degree because the rates are usually calculated by counting the number of events whose strengths exceed a fixed threshold. Hence, we expect poor correlation between MSTID strength and Poynting flux magnitude. The examples given in *Burke et al.* [2016, Figure 6] show that in situ plasma density variations related to MSTIDs are not always correlated with *E* field fluctuation levels, implying similarly poor correlation between plasma density variations and Poynting flux ($= \delta\vec{E} \times \delta\vec{B}/\mu_0$). In situ density fluctuation levels (both absolute and relative levels) along our MMF events are also poorly correlated with the Poynting flux magnitude (figure not shown). In summary, the magnitude of Poynting flux does not seem to reliably represent the MSTID strengths at *F* region altitudes.

In addition to the MSTID strength other parameters may also control the MEF and MMF strengths and corresponding Poynting flux. For example, *Otsuka et al.* [2007, equation 4] showed that MEF amplitudes depend as much on background wind and electric field as on MSTID strength. Note that the equation was derived by a simple requirement for two-dimensional current continuity on the plane perpendicular to background *B* field (i.e., without considering field-aligned currents and related MMFs). If effects of field-aligned currents on three-dimensional current continuity are properly considered, additional parameters are expected to participate in controlling MEF/MMF strengths and resultant Poynting flux magnitudes. It will further complicate the relationship between the MSTID strength and Poynting flux, as Swarm observation results in this study imply. In addition, the feedback from *E* field changes to in situ plasma density variations should also be considered. As one of the referees (M. C. Kelley) pointed out, the correlation between the *E*/*B* field and in situ plasma density can also be affected by vertical motion of the plasma density layer and concomitantly enhanced or reduced recombination of plasma along the *B* field lines.

5. Summary and Conclusion

This is the first statistical survey of MSTID-related field fluctuations, which considers electric field, magnetic field, and plasma density variations at the same time. We have statistically analyzed the direction and magnitude of Poynting flux related to MMFs in the nighttime topside ionosphere. Here MMFs are considered as indicators for MSTIDs. Satellite observations by Swarm-Alpha and Swarm-Bravo were used from about 200 days between 13 December 2013 and 18 March 2015. Our main conclusions can be summarized as follows:

1. During solstices the MMF Poynting flux is preferentially (but not always) from summer to winter hemisphere. During equinoxes there is no preferred direction.
2. Magnitudes of the MMF Poynting flux peak around 2000–2100 MLT and are larger before midnight than after.
3. The magnitudes of the MMF Poynting flux is not well correlated with the undulation levels of in situ plasma density.

Items 1 and 2 can be easily explained in terms of sporadic *E* occurrence, which has been deemed as an essential part of MSTID (and concomitant MEF/MMF) generation by theoretical studies such as *Yokoyama et al.* [2009]. Item 3 can be explained by effects of background parameters (e.g., wind and *E* field) on MEF/MMF amplitudes, as shown by *Otsuka et al.* [2007, equation 4].

Note that our study is based on a limited data set from the Swarm constellation (less than 250 days per satellite) around the year 2014 (near the second peak of solar activity in Solar Cycle 24). The data coverage is especially poor around December solstice. Future studies with a similar approach but based on an extended data set are highly warranted in order to test, for example, (1) if adequate conclusions can be retrieved for other seasons than June solstice and (2) whether similar results can be obtained during deep solar minima.

Acknowledgments
The authors appreciate valuable discussions with Y. Otsuka about MEF/MMF Poynting flux, fruitful e-mail exchanges with T. Yokoyama about MMF theories and helpful comments from the reviewers. The European Space Agency (ESA) is acknowledged for providing the Swarm data. The Swarm data are accessible via https://earth.esa.int/web/guest/swarm/data-access. J.P. was supported by the "Planetary system research for space exploration" project, the basic research funding from KASI, and the Air Force Research Laboratory, under agreement FA2386-14-1-4004. J.K.B. was supported by a Canadian Space Agency grant.

References

Amorim, D. C. M., A. A. Pimenta, J. A. Bittencourt, and P. R. Fagundes (2011), Long-term study of medium-scale traveling ionospheric disturbances using OI 630 nm all-sky imaging and ionosonde over Brazilian low latitudes, *J. Geophys. Res.*, *116*, A06312, doi:10.1029/2010JA016090.

Archer, W. E., D. J. Knudsen, J. K. Burchill, M. R. Patrick, and J. P. St. Maurice (2015), Anisotropic core ion temperatures associated with strong zonal flows and upflows, *Geophys. Res. Lett.*, *42*(4), 981–986, doi:10.1002/2014GL062695.

Arras, C. (2010), A global survey of sporadic *E* layers based on GPS radio occultations by CHAMP, GRACE and FORMOSAT-3/COSMIC, PhD thesis, Scientific Technical Report ; 10/09, Potsdam: Deutsches GeoForschungsZentrum GFZ.

Arras, C., J. Wickert, G. Beyerle, S. Heise, T. Schmidt, and C. Jacobi (2008), A global climatology of ionospheric irregularities derived from GPS radio occultation, *Geophys. Res. Lett.*, *35*, L14809, doi:10.1029/2008GL034158.

Behnke, R. (1979), *F* layer height bands in the nocturnal ionosphere over Arecibo, *J. Geophys. Res.*, *84*(A3), 974–978, doi:10.1029/JA084iA03p00974.

Burke, W. J., C. R. Martinis, P. C. Lai, L. C. Gentile, C. Sullivan, and R. F. Pfaff (2016), C/NOFS observations of electromagnetic coupling between magnetically conjugate MSTID structures, *J. Geophys. Res. Space Physics*, *121*, 2569–2582, doi:10.1002/2015JA021965.

Cosgrove, R. B., and R. T. Tsunoda (2004), Instability of the *E*-*F* coupled nighttime midlatitude ionosphere, *J. Geophys. Res.*, *109*, A04305, doi:10.1029/2003JA010243.

Fiori, R. A. K., D. Boteler, D. Knudsen, and J. Burchill (2016), Calibration and assessment of Swarm ion drift measurements using a comparison with a statistical convection model, *Earth Planet Space*, *68*, 100, doi:10.1186/s40623-016-0472-7.

Garcia, R. F., S. Bruinsma, L. Massarweh, and E. Doornbos (2016), Medium-scale gravity wave activity in the thermosphere inferred from GOCE data, *J. Geophys. Res. Space Physics*, *121*, 8089–8102, doi:10.1002/2016JA022797.

Goodwin, L. V., et al. (2015), Swarm in situ observations of *F* region polar cap patches created by cusp precipitation, *Geophys. Res. Lett.*, *42*, 996–1003, doi:10.1002/2014GL062610.

Hatch, S. M., C. C. Chaston, and J. LaBelle (2016), Alfvén wave-driven ionospheric mass outflow and electron precipitation during storms, *J. Geophys. Res. Space Physics*, *121*, 7828–7846, doi:10.1002/2016JA022805.

Hernández-Pajares, M., J. M. Juan, J. Sanz, and Aragón-Àngel A. (2012), Propagation of medium scale traveling ionospheric disturbances at different latitudes and solar cycle conditions, *Radio Sci.*, *47*, RS0K05, doi:10.1029/2011RS004951.

Juusola, L., W. Archer, K. Kauristie, J. Burchill, H. Vanhamaki, and A. Aikio (2016), Ionospheric conductances and currents of a morning-sector auroral arc from Swarm-A electric and magnetic field measurements, *J. Geophys. Res. Space Physics*, doi:10.1002/2016GL070248, in press.

Kelley, M. C., D. J. Knudsen, and J. F. Vickrey (1991), Poynting flux measurements on a satellite: A diagnostic tool for space research, *J. Geophys. Res.*, *96*(A1), 201–207, doi:10.1029/90JA01837.

Kelley, M. C. (2009), *The Earth's ionosphere: Plasma physics and electrodynamics*, International Geophysics Series, vol. 43, Acad. Press, San, Diego.

Knudsen, D., J. Burchill, S. Buchert, I. Coco, L. Toffner-Clausen, and P. E. Holmdahl Olsen (2014), *Swarm Preliminary Plasma Dataset User Note*, SWAM-GSEG-EOPG-TN-15-0003, pp. 2–12, Frascati, Italy.

Lühr, H., M. Rother, S. Maus, W. Mai, and D. Cooke (2003), The diamagnetic effect of the equatorial Appleton anomaly: Its characteristics and impact on geomagnetic field modeling, *Geophys. Res. Lett.*, *30*, 1906, doi:10.1029/2003GL017407.

Lühr, H., J. Park, J. W. Gjerloev, J. Rauberg, I. Michaelis, J. M. G. Merayo, and P. Brauer (2015), Field-aligned currents' scale analysis performed with the Swarm constellation, *Geophys. Res. Lett.*, *42*, 1–8, doi:10.1002/2014GL062453.

Makela, J. J., E. S. Miller, and E. R. Talaat (2010), Nighttime medium-scale traveling ionospheric disturbances at low geomagnetic latitudes, *Geophys. Res. Lett.*, *37*, L24104, doi:10.1029/2010GL045922.

Martinis, C., J. Baumgardner, J. Wroten, and M. Mendillo (2010), Seasonal dependence of MSTIDs obtained from 630.0 nm airglow imaging at Arecibo, *Geophys. Res. Lett.*, *37*, L11103, doi:10.1029/2010GL043569.

Otsuka, Y., K. Shiokawa, T. Ogawa, and P. Wilkinson (2004), Geomagnetic conjugate observations of medium-scale traveling ionospheric disturbances at midlatitude using all-sky airglow imagers, *Geophys. Res. Lett.*, *31*, L15803, doi:10.1029/2004GL020262.

Otsuka, Y., F. Onoma, K. Shiokawa, T. Ogawa, M. Yamamoto, and S. Fukao (2007), Simultaneous observations of nighttime medium-scale traveling ionospheric disturbances and *E* region field-aligned irregularities at midlatitude, *J. Geophys. Res.*, *112*, A06317, doi:10.1029/2005JA011548.

Otsuka, Y., K. Suzuki, S. Nakagawa, M. Nishioka, K. Shiokawa, and andT. Tsugawa (2013), GPS observations of medium-scale traveling ionospheric disturbances over Europe, *Ann. Geophys.*, *31*, 163–172, doi:10.5194/angeo-31-163-2013.

Park, J., H. Lühr, C. Stolle, M. Rother, K. W. Min, J.-K. Chung, Y. H. Kim, I. Michaelis, and M. Noja (2009), Magnetic signatures of medium-scale traveling ionospheric disturbances as observed by CHAMP, *J. Geophys. Res.*, *114*, A03307, doi:10.1029/2008JA013792.

Park, J., H. Lühr, G. Kervalishvili, J. Rauberg, I. Michaelis, C. Stolle, and Y.-S. Kwak (2015), Nighttime magnetic field fluctuations in the topside ionosphere at midlatitudes and their relation to medium-scale traveling ionospheric disturbances: The spatial structure and scale sizes, *J. Geophys. Res. Space Physics*, *120*, 6818–6830, doi:10.1002/2015JA021315.

Saito, A., T. Iyemori, M. Sugiura, N. C. Maynard, T. L. Aggson, L. H. Brace, M. Takeda, and M. Yamamoto (1995), Conjugate occurrence of the electric field fluctuations in the nighttime midlatitude ionosphere, *J. Geophys. Res.*, *100*(A11), 21439.

Saito, A., T. Iyemori, L. G. Blomberg, M. Yamamoto, and M. Takeda (1998), Conjugate observations of the mid-latitude electric field fluctuations with the MU radar and the Freja satellite, *J. Atmos. Sol. Terr. Phys.*, *60*, 129–140.

Shiokawa, K., Y. Otsuka, C. Ihara, T. Ogawa, and F. J. Rich (2003a), Ground and satellite observations of nighttime medium-scale traveling ionospheric disturbance at midlatitude, *J. Geophys. Res.*, *108*, 1145, doi:10.1029/2002JA009639.

Shiokawa, K., C. Ihara, Y. Otsuka, and T. Ogawa (2003b), Statistical study of nighttime medium-scale traveling ionospheric disturbances using midlatitude airglow images, *J. Geophys. Res.*, *108*, 1052, doi:10.1029/2002JA009491.

Stolle, C., H. Lühr, M. Rother, and G. Balasis (2006), Magnetic signatures of equatorial spread *F*, as observed by the CHAMP satellite, *J. Geophys. Res.*, *111*, A02304, doi:10.1029/2005JA011184.

Tsunoda, R. T. (2006), On the coupling of layer instabilities in the nighttime midlatitude ionosphere, *J. Geophys. Res.*, *111*, A11304, doi:10.1029/2006JA011630.

Xiong, C., J. Park, H. Lühr, C. Stolle, and S. Y. Ma (2010), Comparing plasma bubble occurrence rates at CHAMP and GRACE altitudes during high and low solar activity, *Ann. Geophys.*, *28*(9), 1647–1658, doi:10.5194/angeo-28-1647-2010.

Xiong, C., C. Stolle, H. Lühr, J. Park, B. G. Fejer, and G. N. Kervalishvili (2016), Scale analysis of equatorial plasma irregularities derived from Swarm constellation, *Earth, Planets and Space*, *68*, 121, doi:10.1186/s40623-016-0502-5.

Yokoyama, T., and C. Stolle (2016), Low and Midlatitude Ionospheric Plasma Density Irregularities and Their Effects on Geomagnetic Field, *Space Sci. Rev.*, 1–25, doi:10.1007/s11214-016-0295-7.

Yokoyama, T., D. L. Hysell, Y. Otsuka, and M. Yamamoto (2009), Three-dimensional simulation of the coupled Perkins and E_S-layer instabilities in the nighttime midlatitude ionosphere, *J. Geophys. Res.*, *114*, A03308, doi:10.1029/2008JA013789.

Yokoyama, T. (2014), Hemisphere-coupled modeling of nighttime medium-scale traveling ionospheric disturbances, *Adv. Space Res.*, *54*(3), 481–488, doi:10.1016/j.asr.2013.07.048.